Stoichiometry and Architecture of Active DNA Replication Machinery in Escherichia coli

Rodrigo Reyes-Lamothe, *et al.*

Science **328**, 498 (2010);
DOI: 10.1126/science.1185757

Stoichiometry and Architecture of Active DNA Replication Machinery in *Escherichia coli*

Rodrigo Reyes-Lamothe,[1] David J. Sherratt,[1] Mark C. Leake[1,2]*

The multiprotein replisome complex that replicates DNA has been extensively characterized in vitro, but its composition and architecture in vivo is unknown. Using millisecond single-molecule fluorescence microscopy in living cells expressing fluorescent derivatives of replisome components, we have examined replisome stoichiometry and architecture. Active *Escherichia coli* replisomes contain three molecules of the replicative polymerase, rather than the historically accepted two. These are associated with three molecules of τ, a clamp loader component that trimerizes polymerase. Only two of the three sliding clamps are always associated with the core replisome. Single-strand binding protein has a broader spatial distribution than the core components, with 5 to 11 tetramers per replisome. This in vivo technique could provide single-molecule insight into other molecular machines.

Replisomes are dynamic multiprotein machines that replicate DNA by copying the leading-strand template continuously and the lagging-strand template discontinuously. In *E. coli* the replisome couples the activities of more than 11 proteins during genome replication (*1*, *2*). The DnaB helicase, loaded onto the lagging-strand template, separates the two templates that are subsequently copied by Pol III polymerase (αεθ). Pol III processivity results from binding to a sliding clamp (β) encircling duplex DNA; sliding clamps are added and removed by a clamp loader [$(\tau/\gamma)_3\delta\delta'\psi\chi$] whose τ component oligomerizes Pol III. Unwound DNA on the lagging-strand template is bound by single-strand binding protein (Ssb) tetramers that remove DNA secondary structure and protect against nucleases. Primase binds to helicase during cycles of priming and DNA synthesis on the lagging-strand template.

In vitro studies of the replisome have yielded details of replisome organization and the replication mechanism but have not revealed how replication is organized within living cells. Additional copies of known replisome components may be present at replication forks, whereas additional cellular factors, absent from in vitro assays, may modify the composition of the replisome and act in DNA processing. Furthermore, the techniques used to determine stoichiometry and architecture in vitro favor strong interactions, potentially biasing estimates on numbers and interactions, and are subject to complications if any component is proteolytically sensitive. We thus investigated active replisome architecture in living cells by means of a fluorescence microscopy protocol with single-molecule sensitivity and millisecond temporal resolution.

Using fully functional fluorescent C- or N-terminal YPet derivatives of *E. coli* replisome components expressed from their endogenous promoters, we showed previously that the two spatially separable sister replisomes derived from a single initiation event at the replication origin, *oriC*, track independently along DNA (*3*). Using these and additional fusions, we analyzed 10 components of individual replisomes by "slimfield" fluorescence microscopy, which uses a compact Gaussian laser excitation field (~30 μm^2) that encompasses single cells with an excitation intensity ~100 times that of wide-field fluorescence (*4*, *5*). This imaging allows quantitative detection of single fluorescent molecules at 3-ms capture rates (Fig. 1, A and B). The high laser excitation intensity does not abolish DNA replication, as judged by a factor of 2 difference in turnover on DNA of Ssb-YPet in replicating and nonreplicating cells exposed to an excitation intensity and duration similar to that of slimfield microscopy (fig. S1), consistent with the demonstration that similar exposures do not inhibit flagellar rotation (*4*).

For estimation of stoichiometry, image frames were averaged over 90 ms to define "regions of interest" that are hotspots for localization of a given YPet fusion protein. The position, size, shape, and intensity of the spots were measured automatically for each individual image frame, generating step-like intensity traces as photobleaching occurred (Fig. 1, D and E). We measured the step spacing with the use of an edge-preserving filter (*6*, *7*) combined with Fourier spectral analysis and compared these with intensity traces from purified YPet in vitro (*8*–*10*); the in vivo steps were

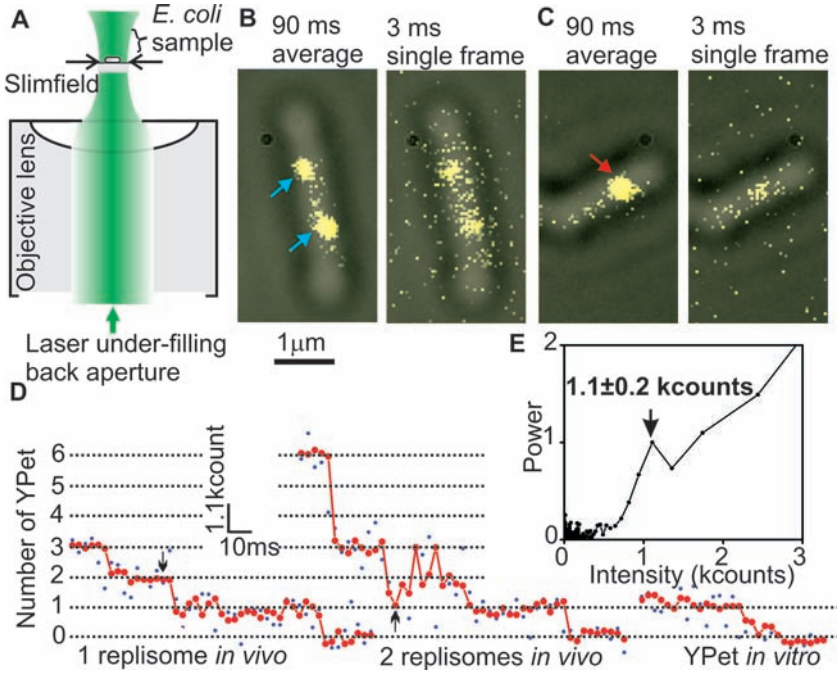

Fig. 1. Slimfield microscopy and photobleach analysis. (**A**) Slimfield schematic. A laser underfills the back aperture of an objective lens, generating an intense Gaussian field at the sample large enough to image single *E. coli*. (**B** and **C**) Overlaid bright-field (gray) and 90-ms frame-averaged fluorescence images (yellow) of ε-YPet strain; arrows indicate spots with a stoichiometry of ~3 [cyan, (B)] and ~6 [red, (C)] ε-YPet molecules, with corresponding single 3-ms frames taken after 45 ms, showing that stochastic photobleaching generates different brightnesses. (**D**) Raw intensity (blue) and filtered data (red) for a putative single (left panel) and double (right panel) replisome spot with surface-immobilized YPet in vitro; arrows indicate the 45-ms point. (**E**) Fourier spectral analysis for a photobleach trace of the ε-YPet strain with mean ± SD peak indicated for brightness of a single YPet.

[1]Department of Biochemistry, University of Oxford, Oxford OX1 3QU, UK. [2]Department of Physics, University of Oxford, Oxford OX1 3PU, UK.

*To whom correspondence should be addressed. E-mail: m.leake1@physics.ox.ac.uk

approximately integer multiples of the in vitro intensity of a single YPet molecule (*4*, *5*, *8*–*13*). Thus, intensities prior to photobleaching enabled single-molecule stoichiometry determination (*5*).

For most replisome components, we observed bimodal 1:2 distributions of stoichiometries, reflecting the observation that ~75% of cells contain two spatially separated replisomes, each associated with independent forks, while ~25% have sister replisomes separated by a distance smaller than the diffraction limit of our system (~250 nm) and are thus observed as a single spot (*3*). Lower stoichiometries were always associated with spots from cells containing two spots; cells with a single spot displayed doubled stoichiometries (Fig. 2). With the ε-YPet strain we observed a bimodal distribution with two Gaussians, peaks centered on 2.9 ± 1.0 (mean ± SD, SEM ~ 0.2) and 6.0 ± 1.3 molecules, consistent with a model in which a single fork contains three copies of ε, the proofreading exonuclease of the core polymerase. The Pol III catalytic subunit, α, had a bimodal distribution with peaks centered on 3.1 ± 1.1 and 5.8 ± 1.1 molecules. Similarly, the clamp loader component, τ, which also oligomerizes the polymerase, had peaks at 3.1 ± 0.8 and 5.6 ± 0.8 molecules. An essential component of the clamp loader, δ, expected to be present in one copy, had peaks at 1.0 ± 0.4 and 2.0 ± 0.4 molecules. Furthermore, we observed a stoichiometry of ~6 and ~12 molecules for DnaB (fig. S2), as expected for the hexameric helicase.

Nonessential χ and ψ, which heterodimerize, have been reported to be present at one copy per replisome because of ψ binding to γ/τ in the clamp loader (*1*, *14*). Instead, we found a mean of ~4 copies per single replisome spot (Fig. 2); single-spot cells had ~8 molecules per spot, with a broader distribution of stoichiometries than for other low-copy components. We propose that this results from one χψ heterodimer being tethered to the clamp loader while the other χψ dimers bind available C-terminal tails of the same or different Ssb tetramers by a characterized interaction through χ (*14*). The intensity of ψ-YPet foci is greatly reduced when χ is absent, but χ focus intensity is unchanged when ψ is absent, supporting this hypothesis (fig. S3).

dnaX expresses comparable amounts of τ and a truncated form, γ, formed by a programmed frameshift (*15*); τ and γ can interchangeably be clamp loader constituents, but only τ oligomerizes Pol III (*1*). Our demonstration that three copies of τ are associated with the replisome suggests that γ is not associated with the single clamp loader in most replisomes. To test this, we constructed two strains: *dnaX*(γ⁻), which did not express γ because the frameshift was abrogated, and *dnaX*(γ-YPet), which expressed γ-YPet. The strain that failed to express γ grew well, confirming that γ is nonessential (*16*), while the strain expressing γ-YPet showed fluorescent replisome-associated foci (fig. S4A). Because γ can interact with χψ, we considered whether γ might be Ssb-associated via a linking interaction

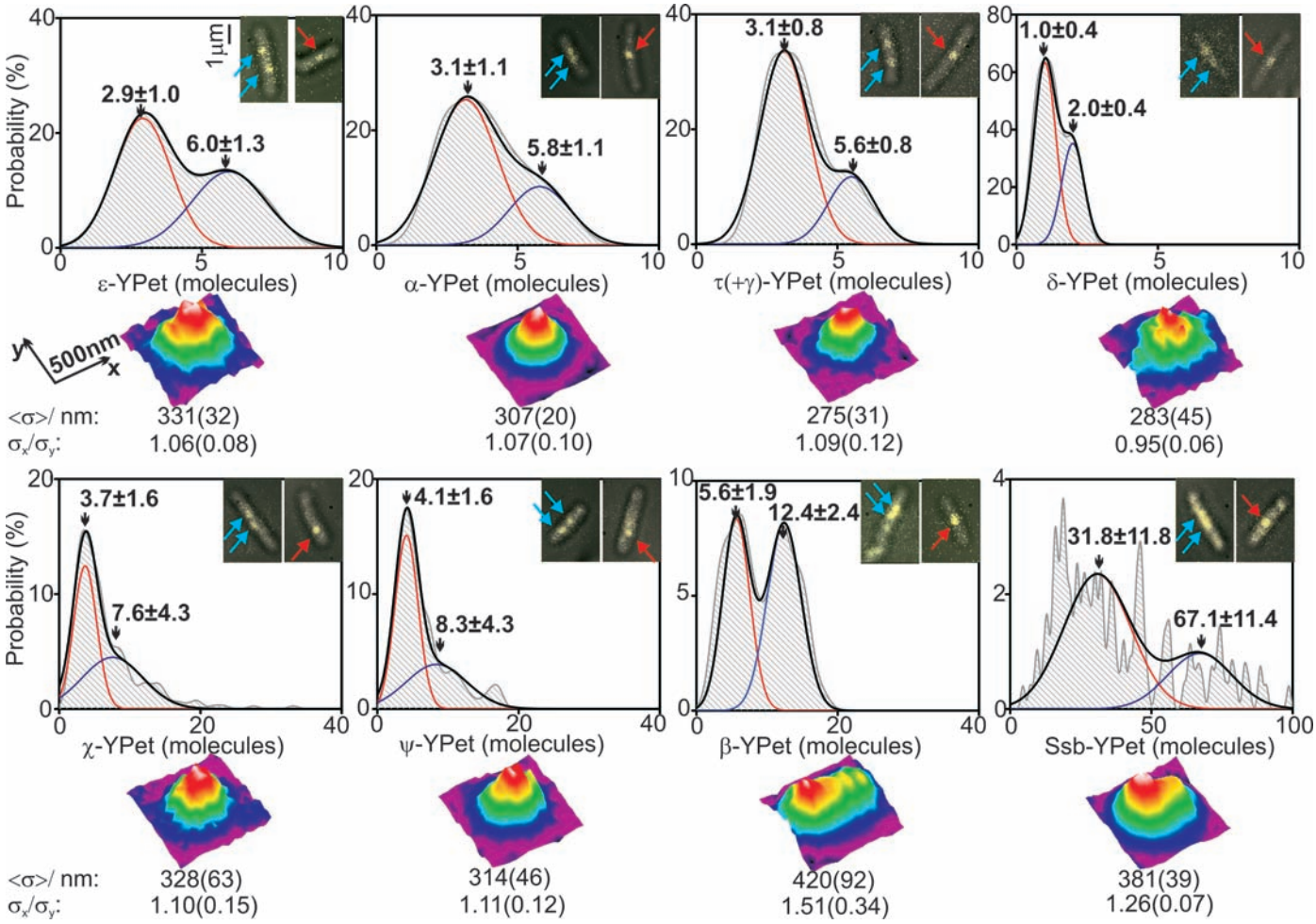

Fig. 2. Stoichiometries of replisome components and spatial distributions. Upper panels: Stoichiometry distributions per spot, using unbiased kernel density estimation for different *E. coli* strains (*N* = 27 to 51 cells in each data set); shown are two-Gaussian fits (black) with contributing single-Gaussian curves (red and blue) and mean ± SD of Gaussian peaks. Insets show examples of overlaid bright-field (gray) and single 3-ms fluorescence images (yellow) for each; arrows indicate foci in cells containing two (cyan) and one (red) replisome. Lower panels: False-color contour plots for 2D averaged spatial distributions for each strain (*N* = 42 to 151 spots in each data set). Estimates for mean FWHM ⟨σ⟩ of a symmetrical 2D Gaussian fit and the ratio σ_x/σ_y of the FWHM for the 1D Gaussian fits through the mean spot parallel to the *x* and *y* axes are indicated; SD errors are in parentheses.

with the χψ heterodimers not associated with the clamp loader (Fig. 3). Targeted proteolysis of degron-tagged ψ, or deletion of χ or ψ, led to a loss of replisome-associated γ-YPet foci, but not ε-YPet or τ-YPet foci; the remaining γ-YPet foci were of reduced intensity (fig. S4B). Thus, the single replicative clamp loader in each replisome contains τ but not γ, and the clamp loader–independent copies of χψ associated with Ssb are likely to recruit γ to Ssb in addition to acting in primase release (*17*). We propose that γ may replace τ as a clamp loader component in postreplication repair-associated events at the replication fork. Comparison of τ stoichiometry in *dnaX* and *dnaX*(γ⁻) strains showed a ~30% increase when γ was absent (fig. S5), indicating that γ and τ can compete for binding to Ssb.

In contrast to the structural skeleton components of the replisome, Ssb showed a broad distribution of stoichiometries (Fig. 2) with a periodicity of ~4 molecules (fig. S6) and a mean of 31.8 ± 11.1 molecules per spot for cells containing two spots per cell, consistent with 8 ± 3 Ssb tetramers per replication fork. Single-spot cells had a stoichiometry larger by a factor of ~2, at ~70 molecules per spot. The number of Ssb molecules bound at the replication fork is expected to be proportional to the length of single-stranded DNA (ssDNA). The average stoichiometry of Ssb within replisomes approximately doubled in cells treated with hydroxyurea (*5*), as expected, because ssDNA accumulates at the fork when replication is stalled (*18*). The ssDNA associated with each Ssb tetramer is either 35 or 65 nucleotides (nt) in vitro; $(Ssb)_{35}$ forms compact filaments, whereas $(Ssb)_{65}$ forms dimers of tetramers covering 170 nt (*19*). The contribution of each binding mode in vivo is unknown. Assuming that the stretch of ssDNA at the replication fork equals the Okazaki fragment length [~650 nt at 22°C (*20*)], then the presence of $(Ssb)_{65}$ would give an occupancy of ~8 tetramers, close to our mean stoichiometry estimate for single replisome spots (Fig. 2).

Structural investigations of replisome components suggest that their cumulative volume is contained in a sphere of maximum diameter ~50 nm (*21*–*24*). To investigate this, we studied the size and shape of images from each strain (Fig. 2, lower panels). Strains expressing fluorescent α, ε, τ, δ, χ, and ψ all produced spots with a circularly symmetrical shape and a mean full width at half maximum (FWHM) across the cell strains of 305 ± 30 nm (*5*). There was no significant difference from the individual FWHM measurements for each strain ($P = 0.05$, Student *t* test), but all were significantly larger than the FWHM of surface-immobilized YPet in vitro of ~250 nm (fig. S7). In contrast, β and Ssb produced spots spread further over the long axis of the cell, with Ssb foci extending up to ~200 nm; ~55% of the tetramers were present within a 50-nm diameter. Although the ~4 χψ heterodimers may interact with Ssb tails, we note that the spatial distribution of χψ is that of the core replisome–clamp loader rather than that of Ssb. Furthermore, the stoichiometry of χψ is much lower than that of Ssb. Taken together, these results suggest that χψ is associated preferentially with one or a few Ssb molecules in the vicinity of the core replisome.

The stoichiometry of the dimeric β sliding clamp was expected to be partly the result of its interaction with Pol III and the clamp loader, and partly due to association with DNA at the 3′ end of Okazaki fragments. Nonetheless, its bimodal distribution peaked at ~3 and ~6 dimers (Fig. 2), which raised the possibility that it might be continually associated with Pol III. Analysis of β-YPet spots indicated two subpopulations with different spatial intensity distributions (fig. S8). The first subgroup (~27% of spots) had circular distributions that support a scheme in which three β dimers are associated with active Pol III or with the clamp loader. In the second subgroup, the spots were more extended (circularity > 1.2), consistent with at least one of the sliding clamps being localized at a distance >50 nm from the replisome core.

Historically, the replisome has been considered to have two opposing yet coordinated polymerases connected to the rest of the replisome (*25*). Instead, we provide strong evidence for an in vivo core replisome containing three Pol IIIs associated with a clamp loader whose three copies of τ also trimerize Pol III. In a minority of replisomes, all three Pol IIIs may be associated with sliding clamps, with two being potentially simultaneously active on the lagging strand, supporting suggestions from in vitro studies of *E. coli* and phage T4 replisomes (*2*, *26*). However, the majority of replisomes appear to have only two of the polymerases associated with a sliding clamp, which suggests that the third polymerase is waiting to be loaded onto the next lagging-strand primer (Fig. 3).

We measured the number of nonreplisome Ssb tetramers to be 330 ± 105 per cell (table S1), in agreement with estimates using quantitative Western blots (*5*). Similarly, 0.5 to 5% of other replisome molecules in a cell were associated with each replisome (table S1), hence the measured stoichiometries reflect biologically relevant complexes and are not the consequence of the replisome's component being rate-limiting. The level of replisome molecules is sufficient to support more than 10 cellular replication forks associated with the chromosome, plasmids, or phage.

Slimfield microscopy provides a powerful noninvasive in vivo analytical tool that extends previous analyses of the assembly and action of molecular machines (*10*, *27*, *28*). In combination with degron-targeted proteolysis of specific proteins, it has provided unanticipated insight into replisome architecture. In combination with partial prebleaching and stochastic photoactivation and photoswitching techniques, the methodology may provide new insight into biological systems that contain substantially higher numbers of freely diffusing fluorescent proteins than were investigated here.

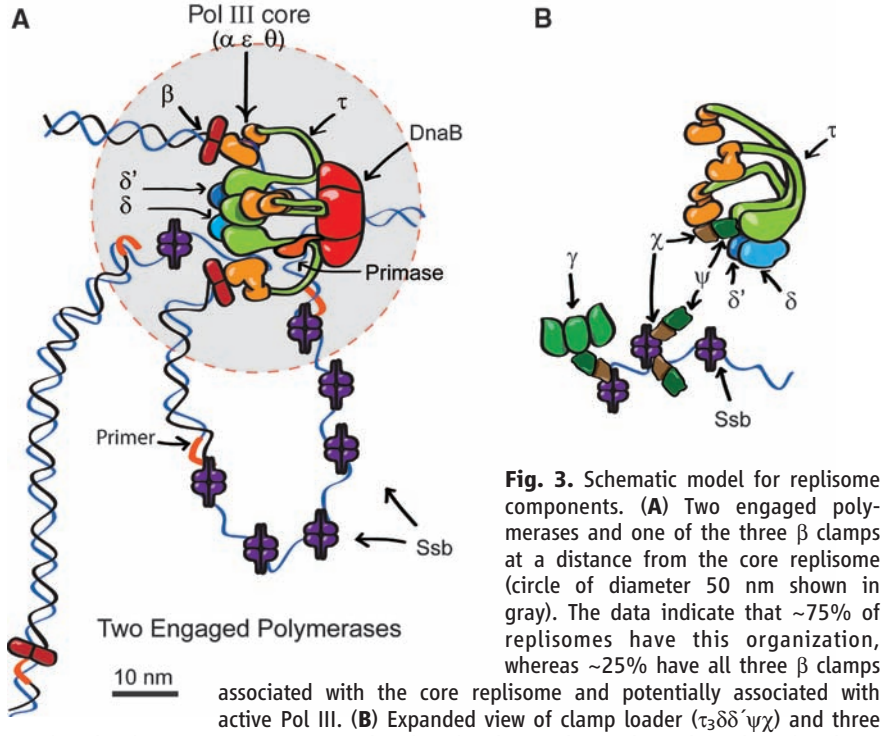

Fig. 3. Schematic model for replisome components. (**A**) Two engaged polymerases and one of the three β clamps at a distance from the core replisome (circle of diameter 50 nm shown in gray). The data indicate that ~75% of replisomes have this organization, whereas ~25% have all three β clamps associated with the core replisome and potentially associated with active Pol III. (**B**) Expanded view of clamp loader ($\tau_3\delta\delta'\psi\chi$) and three additional molecules of χψ interacting with Ssb tails. The χψ heterodimer bound to the clamp loader may also contact Ssb (*14*); γ (shown as a trimer, but the stoichiometry is unknown) then interacts with Ssb-associated χψ.

References and Notes

1. A. Johnson, M. O'Donnell, *Annu. Rev. Biochem.* **74**, 283 (2005).
2. P. McInerney, A. Johnson, F. Katz, M. O'Donnell, *Mol. Cell* **27**, 527 (2007).
3. R. Reyes-Lamothe, C. Possoz, O. Danilova, D. J. Sherratt, *Cell* **133**, 90 (2008).
4. M. Plank, G. H. Wadhams, M. C. Leake, *Integr. Biol.* **1**, 602 (2009).
5. See supporting material on *Science* Online.
6. S. H. Chung, R. A. Kennedy, *J. Neurosci. Methods* **40**, 71 (1991).
7. D. A. Smith, *Philos. Trans. R. Soc. London Ser. B* **353**, 1969 (1998).
8. M. C. Leake, D. Wilson, B. Bullard, R. M. Simmons, *FEBS Lett.* **535**, 55 (2003).
9. M. C. Leake, D. Wilson, M. Gautel, R. M. Simmons, *Biophys. J.* **87**, 1112 (2004).
10. M. C. Leake *et al.*, *Nature* **443**, 355 (2006).
11. M. C. Leake *et al.*, *Proc. Natl. Acad. Sci. U.S.A.* **105**, 15376 (2008).
12. T. Lenn, M. C. Leake, C. W. Mullineaux, *Mol. Microbiol.* **70**, 1397 (2008).
13. T. Lenn, M. C. Leake, C. W. Mullineaux, *Biochem. Soc. Trans.* **36**, 1032 (2008).
14. K. R. Simonetta *et al.*, *Cell* **137**, 659 (2009).
15. A. L. Blinkowa, J. R. Walker, *Nucleic Acids Res.* **18**, 1725 (1990).
16. A. Blinkova *et al.*, *J. Bacteriol.* **175**, 6018 (1993).
17. A. Yuzhakov, Z. Kelman, M. O'Donnell, *Cell* **96**, 153 (1999).
18. P. McInerney, M. O'Donnell, *J. Biol. Chem.* **282**, 25903 (2007).
19. T. M. Lohman, M. E. Ferrari, *Annu. Rev. Biochem.* **63**, 527 (1994).
20. N. Y. Yao, R. E. Georgescu, J. Finkelstein, M. E. O'Donnell, *Proc. Natl. Acad. Sci. U.S.A.* **106**, 13236 (2009).
21. S. L. Kazmirski, M. Podobnik, T. F. Weitze, M. O'Donnell, J. Kuriyan, *Proc. Natl. Acad. Sci. U.S.A.* **101**, 16750 (2004).
22. M. H. Lamers, R. E. Georgescu, S. G. Lee, M. O'Donnell, J. Kuriyan, *Cell* **126**, 881 (2006).
23. R. E. Georgescu *et al.*, *Cell* **132**, 43 (2008).
24. S. Bailey, W. K. Eliason, T. A. Steitz, *Science* **318**, 459 (2007).
25. B. M. Alberts *et al.*, *Cold Spring Harb. Symp. Quant. Biol.* **47**, 655 (1983).
26. N. G. Nossal, A. M. Makhov, P. D. Chastain 2nd, C. E. Jones, J. D. Griffith, *J. Biol. Chem.* **282**, 1098 (2007).
27. X. S. Xie, J. Yu, W. Y. Yang, *Science* **312**, 228 (2006).
28. J. Q. Wu, T. D. Pollard, *Science* **310**, 310 (2005).

29. Supported by the Wellcome Trust and the Royal Society. M.C.L. is a Royal Society University Fellow and research fellow of Hertford College Oxford. R.R.-L. is a research fellow of New College Oxford and was supported by Conacyt and a Clarendon postgraduate award. We thank C. Possoz and C. Lesterlin for stimulating discussions, and we acknowledge National BioResource Project (NIG, Japan): *E. coli* for the provision of the *holC* and *holD* deletion strains.

Supporting Online Material

www.sciencemag.org/cgi/content/full/328/5977/498/DC1
Materials and Methods
Figs. S1 to S11
Table S1
References

9 December 2009; accepted 8 March 2010
10.1126/science.1185757

A NusE:NusG Complex Links Transcription and Translation

Björn M. Burmann,[1] Kristian Schweimer,[1] Xiao Luo,[2] Markus C. Wahl,[2] Barbara L. Stitt,[3] Max E. Gottesman,[4] Paul Rösch[1]*

Bacterial NusG is a highly conserved transcription factor that is required for most Rho activity in vivo. We show by nuclear magnetic resonance spectroscopy that *Escherichia coli* NusG carboxy-terminal domain forms a complex alternatively with Rho or with transcription factor NusE, a protein identical to 30*S* ribosomal protein S10. Because NusG amino-terminal domain contacts RNA polymerase and the NusG carboxyl-terminal domain interaction site of NusE is accessible in the ribosomal 30*S* subunit, NusG may act as a link between transcription and translation. Uncoupling of transcription and translation at the ends of bacterial operons enables transcription termination by Rho factor, and competition between ribosomal NusE and Rho for NusG helps to explain why Rho cannot terminate translated transcripts.

Escherichia coli NusG is a two-domain protein (fig. S1) (*1*) that is essential for cell viability (*2*). NusG homologs are found in all known bacteria, and the 27–amino acid NusG carboxy-terminal domain (CTD) Kyprides-Onzonis-Woese (KOW) motif is found in proteins from archaea and eukaryotes (*3*–*5*). A sequence highly homologous to NusG amino-terminal domain (NTD) followed by KOW motifs appears in human transcription factor hSpt5 (*6*). NusG suppresses RNA polymerase (RNAP) pausing and increases elongation rates in vitro. In vivo, it acts in concert with NusA, NusB, and NusE to promote readthrough of terminators within ribosomal *rrn* operons and on the phage λ chromosome, a process that additionally requires the λ N protein (*7*). NusG activates Rho transcription termination factor in vitro and is necessary for most Rho-mediated termination events in vivo (*8*, *9*). NusG-NTD binds to RNAP and increases the rate of transcription elongation but cannot stimulate termination (*1*, *10*).

The rates of transcription and translation are correlated over a range of different growth rates (*11*), and NusG was suggested to be involved in this correlation (*12*). Thus, depletion of NusG slowed the rate of *lacZ* translation without affecting the rate of *lacZ* transcription elongation (*12*). The dual capacity of NusG to act in transcription as well as in translation is shared by the 30*S* ribosomal subunit protein NusE, which doubles as a component of some transcription elongation complexes (TECs) (*13*). As a transcription factor, NusE is loaded by NusB onto the *boxA* sequence within *nut* RNA (*14*–*16*) and becomes part of an antitermination complex that includes NusA, NusG, and other cellular factors (*7*, *17*). The NusB:NusE:RNA ternary complex is proposed to associate with RNAP through NusE (*7*, *18*).

Genetic evidence supports an interaction between NusG and NusE. Thus, the *nusG4* (*S163F*) mutation restores λ N antitermination in a *nusE71* (*nusEA86D*) strain (*19*). We asked whether this genetic interaction reflects a direct physical contact between the proteins. For all experiments, we used the NusE$^{\Delta loop}$ variant (*15*), referred to here as NusE. NusE$^{\Delta loop}$ is fully active for transcription, although it cannot support translation (fig. S2) (*20*), and its crystal structure is known in the NusB:NusE complex (*15*). We analyzed mixtures of NusG and the NusB:NusE complex by size exclusion chromatography. A mixture of NusB:NusE and NusG eluted earlier from the column than either NusB:NusE or NusG alone (fig. S3) (*20*), consistent with formation of a NusB:NusE:NusG complex. To confirm the interaction and to map contact surfaces, we investigated complex formation by NMR. Titration of isolated ^{15}N-labeled NusG-NTD or NusG-CTD with NusB:NusE complex caused chemical shift changes in the ^{1}H, ^{15}N-HSQC (heteronuclear single quantum coherence) nuclear magnetic resonance (NMR) spectrum of NusG-CTD but not of NusG-NTD (figs. S4 and S5). Reverse labeling (^{15}N-NusE or ^{15}N-NusB and unlabeled NusG-CTD) revealed that NusE is the recognition protein in the NusB:NusE complex (figs S4 and S5), suggesting direct NusG-CTD:NusE interaction.

From the chemical shift changes upon titration, we could estimate the dissociation constant for the NusB:NusE:NusG-CTD (molecular mass of 32.3 kD) interaction as K_d = 50 μM (fig. S6). Comparison of secondary chemical shifts and characteristic nuclear Overhauser enhancement spectroscopy (NOESY) cross-peak patterns of NusB:NusE and NusG-CTD with the corresponding data of the NusB:NusE:NusG-CTD complex revealed no substantial conformational changes in any of the participating proteins, indicating that only minor side chain rearrangements are necessary to form the interaction surfaces (Fig.

[1]Lehrstuhl Biopolymere und Forschungszentrum für Bio-Makromoleküle, Universität Bayreuth, Universitätsstraße 30, 95447 Bayreuth, Germany. [2]Freie Universität Berlin, Fachbereich Biologie-Chemie-Pharmazie, Institut für Chemie und Biochemie, AG Strukturbiochemie, Takustr. 6, 14195 Berlin, Germany. [3]Department of Biochemistry and Fels Institute for Cancer Research and Molecular Biology, Temple University School of Medicine, Philadelphia, PA 19140, USA. [4]Department of Microbiology and Institute of Cancer Research, Columbia University Medical Center, New York, NY 10032, USA.

*To whom correspondence should be addressed. E-mail: roesch@unibt.de